Nonlinear IHS: A Promising Method for Pan-Sharpening

Morteza Ghahremani, *Member, IEEE*, and Hassan Ghassemian, *Senior Member, IEEE*

***Abstract*—The goal of pan-sharpening is to increase the spatial resolution of multispectral or hyperspectral images using a high-spatial-resolution panchromatic image. The intensity–hue–saturation (IHS) method is one of the most popular pan-sharpening methods. The pan-sharpening framework of the IHS method is simple, efficient, and of high spatial quality. In this letter, we propose a nonlinear IHS method. The main concern of this letter is how to accurately estimate the intensity component. The proposed method approximates the intensity component via local and global synthesis approaches. The WorldView-2 and DEIMOS-2 data are used to evaluate the performance of the proposed method. The experimental results demonstrate that the proposed nonlinear IHS method generates high-quality pan-sharpened multispectral bands in terms of quantitatively and perceptually.**

***Index Terms*—Hyperspectral data, intensity–hue–saturation (IHS), multispectral data, nonlinear, panchromatic data, pan-sharpening.**

I. Introduction

In MOST remote sensing applications, the demand for spectral data with high spatial resolution is increasing. Due to physical and technological constraints on the designation of satellite sensors, providing multispectral or hyperspectral data with high spatial resolution generates high cost (hereupon, the low-spatial-resolution multispectral data are denoted by LRM). Therefore, to compensate the weak spatial resolution of the LRM data, remote sensing satellites provide a complementary high-spatial-resolution panchromatic (HRP) data. Pan-sharpening or remote sensing image fusion is a promising field, whose goal is to enhance the spatial resolution of the spectral bands without distorting the spectral contents [1].

Thus far, a large number of pan-sharpening methods have been presented. Most of them can be classified into four main categories: component-substitution-based methods such as [2]–[4], multiresolution-analysis-based methods such as [5]–[8], model-based methods such as [8]–[10], and reconstruction-based methods such as [1], [8], [11], and [12]. Detailed surveys on pan-sharpening methods can be found in [13]–[15].

Intensity–hue–saturation (IHS) [2], [16]–[20] is one of the most popular and successful component-substitution-based pan-sharpening frameworks. Easy implementation, high spatial resolution, and good spectral preservation are the main advantages of the IHS-based method. The main problem with this method is the high spectral/color distortion when there is a difference between the HRP data and the estimated intensity component. In recent years, several research studies have been presented to mitigate this phenomenon. Rahmani *et al.* [19] proposed a modified IHS method, in which the intensity component is approximated adaptively. We have earlier [1], [8] proposed methods that use a high-resolution intensity component instead of the HRP data in the fusion process; to minimize the spectral distortion, the intensity components are estimated locally. In this letter, we propose a nonlinear IHS method to assuage the spectral distortion. The main contribution of the proposed method is to estimate the intensity component through local and global approaches. We use the HRP image and its degraded version (LRP) simultaneously to estimate adaptive weight vectors (the LRP image is obtained through low-pass filtering and decimating the HRP image by the ratio "ρ," where ρ is the ratio of the spatial resolutions between the LRM and HRP images). The proposed framework will show that it has great potential for handling complex structural information of the HRP data.

The rest of this letter is structured as follows. Section II briefly reviews the IHS methods. The proposed nonlinear IHS method is presented in Section III. Section IV reports the experimental results and discussion, and finally, the conclusions are drawn in Section V.

II. IHS

In 2001, Tu *et al.* [2] expanded the original IHS and IHS-like methods and introduced a new framework for pan-sharpening, which is defined as

$$M_{\mathrm{H}}^{k} = M_{\mathrm{up.}}^{k} + (P_{\mathrm{his.}} - I_{\mathrm{up.}}), \qquad k = 1, \ldots, L \tag{1}$$

where "M_{H}" and "M" are the pan-sharpened and LRM images, respectively; "L" denotes the number of spectral bands; and the subscript "up." denotes the upsampling operator. "$I_{\mathrm{up.}}$" is an upsampled intensity component, which is obtained via

$$I_{\mathrm{up.}} = \sum_{k=1}^{L} \omega_k y_{k,\mathrm{up.}} = \boldsymbol{\omega}^{\mathrm{T}} M_{\mathrm{up.}} \tag{2}$$

and "$P_{\mathrm{his.}}$" are the histogram-matched HRP data obtained through the following equation:

$$P_{\mathrm{his.}} = \frac{\sigma_{I_{\mathrm{up.}}}}{\sigma_P}(P - \mu_P) + \mu_{I_{\mathrm{up.}}} \tag{3}$$

where "σ" and "μ" denote the standard deviation and mean, respectively. Several research studies [16]–[18] have been

Manuscript received March 11, 2016; revised June 5, 2016 and July 24, 2016; accepted July 30, 2016. Date of publication August 24, 2016; date of current version October 12, 2016.

The authors are with the Faculty of Electrical and Computer Engineering, Tarbiat Modares University, Tehran 14155-4843, Iran (e-mail: morteza.ghahremani@modares.ac.ir; morteza.ghahremani.b@gmail.com; ghassemi@modares.ac.ir).

Color versions of one or more of the figures in this paper are available online at http://ieeexplore.ieee.org.

Digital Object Identifier 10.1109/LGRS.2016.2597271

conducted to determine the weight vector in (2). However, these methods assume a predetermined weight vector, and thus, it generates spectral distortion. To overcome this weakness, Rahmani *et al.* [19] proposed a modified IHS method, which is defined as

$$M_{\mathrm{H}}^{k} = M_{\mathrm{up.}}^{k} + \mathbf{E}(P_{\mathrm{his.}} - I_{\mathrm{up.}}), \qquad k = 1, \ldots, L. \tag{4}$$

Here, $\mathbf{E}$ is an edge detector, which is equal to 1 on the edges and equal to 0 off the edges, i.e.,

$$\mathbf{E} = \exp\left(-\frac{\gamma}{|\nabla P|^4 + \varepsilon}\right) \tag{5}$$

where "∇" is the gradient operator, "γ" is a parameter that controls the magnitude on the edges, and "ε" is a small value that enforces a nonzero denominator. In the modified IHS method, the authors assume a nonnegativity constraint on (2) to estimate the weight vector, i.e.,

$$\hat{\boldsymbol{\omega}} = \arg\min_{\boldsymbol{\omega}} \|P_{\mathrm{his.}} - \boldsymbol{\omega}^{\mathrm{T}} M_{\mathrm{up.}}\|_2^2 + \lambda\left(\sum_{k=1}^{L}(\boldsymbol{\omega}_k \geq 0)\right) \tag{6}$$

where $\boldsymbol{\omega} = (\omega_1, \ldots, \omega_L)^{\mathrm{T}}$ is the weight vector (for further details about the modified IHS method, readers are referred to [19]). Other improvement can be found in [20].

III. Proposed Nonlinear IHS Method

The empirical results show that the modified IHS method considerably improves the content of the pan-sharpened products. However, there are three questions about this method. First, as the modified IHS method uses only the global synthesis approach to obtain the intensity component, how can it deal with the local dissimilarities? Thomas *et al.* [13] showed that the global synthesis during pan-sharpening leads to significant spectral distortion because the structural patterns of the remote sensing data are complex. In other words, a global synthesis approach cannot handle local dissimilarities. Second, it is questionable whether the nonnegativity constraint of the modified IHS method is reasonable. Redundancy is a common phenomenon that is often occurred in the spectral data due to the frequency overlaps of the spectral sensors. Thus, a nonnegativity constraint cannot handle this common phenomenon. Finally, there is no specific trend to determine the Lagrangian parameter in (6), which cannot lead to the optimal weight vector. In fact, this method uses a predetermined λ.

To overcome these drawbacks, we introduce two approaches to approximate the intensity component: 1) utilizing a nonlinear synthesis (or local synthesis) approach instead of the common linear one to approximate the intensity component and 2) utilizing a global synthesis approach to make the intensity component at high spatial resolution consonant with its degraded one. We use the energy constraint proposed in our previous research [1], [8] to overcome the second weakness of the modified IHS method. The efficiency of the energy constraint is proved in [1] and [8]. Moreover, we propose a singular value decomposition (SVD) approach to seek the best λ that leads to the optimal weight vector. Another novelty of this letter is to use both the original and upsampled LRM data, as well as both the HRP data and its degraded version, during the weight vector estimation. This procedure makes the weight vector results stable.

A. Nonlinear Synthesis Approach to Approximate the Intensity Component

The intensity component can be approximated as a linear or a nonlinear combination of the spectral bands. As aforementioned, the structural characteristics of the remote sensing satellites data are more complex than those of the natural data; therefore, a nonlinear model can relax the linear one in most of remote sensing applications. To implement the nonlinear model, a possible solution is to partition the data into small subimages/patches and then apply the linear model on each patch. In the following, we describe this approach in more details.

Notation: Let $X^{(i)} = (X_{1,1}, \ldots, X_{1,\beta}, \ldots, X_{\beta,1}, \ldots, X_{\beta,\beta})^{\mathrm{T}}$ and $x^{(i)} = (x_{1,1}, \ldots, x_{1,B}, \ldots, x_{B,1}, \ldots, x_{B,B})^{\mathrm{T}}$ be the ith patches of the HRP image and its degraded version ordered lexicographically as a column vector, respectively; "β" and "B" are the patch sizes of X and x, respectively, where the relationship between them is $\beta = \rho \times B$. The patch size B is typically chosen between 3 and 5. Likewise, $y_k^{(i)}$ and $y_{k,\mathrm{up.}}^{(i)}$ are the ith patches of the original LRM image and its upsampled version by ρ at the kth bands, respectively. Matrices $Y^{(i)} = (y_1^{(i)}, \ldots, y_k^{(i)})^{\mathrm{T}}$ and $Y_{\mathrm{up.}}^{(i)} = (y_{1,\mathrm{up.}}^{(i)}, \ldots, y_{k,\mathrm{up.}}^{(i)})^{\mathrm{T}}$ denote the ith patches of the entire original LRM and upsampled LRM bands, respectively. Finally, $s^{(i)} = (s_{1,1}, \ldots, s_{1,B}, \ldots, s_{B,1}, \ldots, s_{B,B})^{\mathrm{T}}$ and $S^{(i)} = (S_{1,1}, \ldots, S_{1,\beta}, \ldots, S_{\beta,1}, \ldots, S_{\beta,\beta})^{\mathrm{T}}$ are the ith lexicographically ordered patches of the intensity component and its upsampled version, respectively. When tiling an image into patches, a windowing effect is occurred, which can be resolved by the overlapping approach. In the reconstructing process of the image, we utilize the smooth window presented in [1] instead of the conventional averaging approach in the overlapped regions (for further details about the smooth window, readers are referred to [1]). The total number of patches in the intensity component is denoted by "N."

For each patch $i, i \in \{1, \ldots, N\}$, we apply the linear model on the LRM patches to form the intensity component patches, i.e.,

$$s^{(i)} = \sum_{k=1}^{L} \omega_k^{(i)} y_k^{(i)} = \boldsymbol{\omega}^{(i),\mathrm{T}} Y^{(i)} \tag{7}$$

$$S^{(i)} = \sum_{k=1}^{L} \omega_k^{(i)} y_{k,\mathrm{up.}}^{(i)} = \boldsymbol{\omega}^{(i),\mathrm{T}} Y_{\mathrm{up.}}^{(i)}. \tag{8}$$

To minimize the spectral distortion, the intensity component should approximate the HRP data as closely as possible. To do this, we form the following optimization problem:

$$\hat{\boldsymbol{\omega}}^{(i)} = \arg\min_{\boldsymbol{\omega}^{(i)}} \left\{ \left\| \tilde{X}^{(i)} - \boldsymbol{\omega}^{(i),\mathrm{T}} \tilde{Y}^{(i)} \right\|_2^2 \right\} \text{ s.t. } \boldsymbol{\omega}^{(i),\mathrm{T}} \boldsymbol{\omega}^{(i)} = 1 \tag{9}$$

where

$$\tilde{\mathrm{X}}^{(i)} = \begin{bmatrix} X^{(i)} \\ x^{(i)} \end{bmatrix} \quad \tilde{Y}^{(i)} = \begin{bmatrix} Y_{\mathrm{up.}}^{(i)} \\ Y^{(i)} \end{bmatrix}. \tag{10}$$

In (9), the energy constraint term determines the energy level of each spectral band involved in the intensity component approximation. This constraint is favorable to overcome the redundancy of the remote sensing data and to better investigate

the local dissimilarities. As shown in (10), we stack the input data to have a stable weight vector. The Lagrangian multiplier offers an equivalent formulation to (9), i.e.,

$$\Omega\left(\boldsymbol{\omega}^{(i)},\lambda^{(i)}\right)=\left\|\tilde{X}^{(i)}-\boldsymbol{\omega}^{(i),\mathrm{T}}\tilde{Y}^{(i)}\right\|_2^2+\lambda^{(i)}\left(\boldsymbol{\omega}^{(i),\mathrm{T}}\boldsymbol{\omega}^{(i)}-1\right) \tag{11}$$

where $\lambda \geq 0$ is a Lagrangian multiplier that plays the role of a dual variable. Minimizing $\Omega(\boldsymbol{\omega}^{(i)},\lambda^{(i)})$ over $\boldsymbol{\omega}^{(i)}$, we can obtain the Lagrangian dual

$$\Gamma(\lambda^{(i)})=\arg\min_{\boldsymbol{\omega}^{(i)}}\ \Omega(\boldsymbol{\omega}^{(i)},\lambda^{(i)})=\tilde{X}^{(i),\mathrm{T}}\tilde{X}^{(i)} - (\tilde{Y}^{(i),\mathrm{T}}\tilde{X}^{(i)})^{\mathrm{T}}(\tilde{Y}^{(i),\mathrm{T}}\tilde{Y}^{(i)}+\lambda^{(i)}\mathbf{I})^{-1}\tilde{Y}^{(i),\mathrm{T}}\tilde{X}^{(i)} \tag{12}$$

where "$\mathbf{I}$" is an identity matrix of size "L." The gradient of $\Gamma(\lambda)$ for the ith patch can be computed as follows:

$$\frac{d}{d\lambda^{(i)}}\Gamma\left(\lambda^{(i)}\right)=\left\|\tilde{X}^{(i),\mathrm{T}}\tilde{Y}^{(i)}(\tilde{Y}^{(i),\mathrm{T}}\tilde{Y}^{(i)}+\lambda^{(i)}\mathbf{I})^{-1}\right\|_2^2-1 \tag{13}$$

$$\frac{d^2}{d\lambda^{(i),2}}\Gamma(\lambda^{(i)})=-2\tilde{Y}^{(i),T}\tilde{X}^{(i)}\left(\tilde{Y}^{(i),T}\tilde{Y}^{(i)}+\lambda^{(i)}\mathbf{I}\right)^{-1} \times\left\{\left(\tilde{Y}^{(i),T}\tilde{Y}^{(i)}+\lambda^{(i)}\mathbf{I}\right)^{-1}\left(\tilde{Y}^{(i),T}\tilde{X}^{(i)}\right) \times\left(\tilde{Y}^{(i),T}\tilde{X}^{(i)}\right)^{T}\left(\tilde{Y}^{(i),T}\tilde{Y}^{(i)}+\lambda^{(i)}\mathbf{I}\right)^{-1}\right\}. \tag{14}$$

Now, we optimize the Lagrange dual using Newton's method. After maximizing, we obtain the optimal weight vector ω as follows:

$$\hat{\boldsymbol{\omega}}^{(i)}=\left(\tilde{Y}^{(i),\mathrm{T}}\tilde{Y}^{(i)}+\hat{\lambda}^{(i)}\mathbf{I}\right)^{-1}\tilde{Y}^{(i),\mathrm{T}}\tilde{X}^{(i)} \qquad \forall\, i=1,\ldots,N. \tag{15}$$

A fast implementation of the weight vector estimator can be done through the SVD approach [21]. The details of the ω estimator are presented in Fig. 1. Inserting $\hat{\boldsymbol{\omega}}^{(i)}$ into (7) and (8) gives us $s^{(i)}$ and $S^{(i)}$, respectively. We use the smooth window in the overlapped regions to generate the intensity component I and the initial upsampled intensity component $I_{0,\mathrm{up.}}$.

B. Global Synthesis of the Intensity Component

The intensity components obtained through the local synthesis approach, i.e., I and $I_{0,\mathrm{up.}}$, may not satisfy the global reconstruction, i.e., $I=\mathbf{M}I_{\mathrm{up.}}$, exactly, where "$\mathbf{M}$" is the downscaling operator. We can eliminate this effect by

$$\hat{I}_{\mathrm{up.}}=\arg\min_{I_{\mathrm{up.}}}\ \|I-\mathbf{M}I_{\mathrm{up.}}\|_2^2+\eta\|I_{\mathrm{up.}}-I_{0,\mathrm{up.}}\|_2^2 \tag{16}$$

where "η" is a parameter used to balance the reconstruction constraint fidelity and the initial estimated intensity component given by the local synthesis approach, which is set as 1. Gradient descent is a possible solution to this optimization problem. The updated equation for this iterative method is

$$I_{\mathrm{up.}}^{t+1}=I_{\mathrm{up.}}^{t}+\upsilon\left[\mathbf{M}^{T}\left(I-\mathbf{M}I_{\mathrm{up.}}^{t}\right)+\eta\left(I_{\mathrm{up.}}^{t}-I_{0,\mathrm{up.}}\right)\right]. \tag{17}$$

Algorithm 1: Approximate the Solution of (9)

Input:

$\tilde{\mathrm{Y}}$ - the spectral information patches,

$\tilde{\mathrm{X}}$ - the spatial information patches,

N- total number of patches, and

For each patch i, $i\in\{1,...,N\}$,

1. Compute $\mathrm{SVD}(\tilde{\mathrm{Y}}^{(i)})=U^{(i)}\Sigma^{(i)}V^{(i),\mathrm{T}}=\sum_{j=1}^{L}\sigma_j^{(i)}u_j^{(i)}v_j^{(i),\mathrm{T}}$.

2. if $\sum_{j=1}^{L}\left(\frac{u_j^{(i)}\tilde{\mathrm{X}}^{(i)}}{\sigma_j^{(i)}}\right)^2=1$, then

$$\hat{\boldsymbol{\omega}}^{(i)}=\sum_{j=1}^{L}\left(\frac{u_j^{(i)}\tilde{\mathrm{X}}^{(i)}}{\sigma_j^{(i)}}\right)v_j^{(i)}$$

else

Apply Newton's method to find $\lambda_+^{(i)}$ such that $\sum_{j=1}^{L}\left(\frac{\sigma_j^{(i)}u_j^{(i)}\tilde{\mathrm{X}}^{(i)}}{\sigma_j^{(i),2}+\lambda_+^{(i)}}\right)^2=1$.

$$\hat{\boldsymbol{\omega}}^{(i)}=\sum_{j=1}^{L}\left(\frac{\sigma_j^{(i)}u_j^{(i)}\tilde{\mathrm{X}}^{(i)}}{\sigma_j^{(i),2}+\lambda_+^{(i)}}\right)v^{(i)}$$

end

Output: The desired result is $\hat{\boldsymbol{\omega}}^{(i)}$, $i\in\{1,...,N\}$.

Fig. 1. Proposed fast weight vector estimator used for solving (9).

Here, $I_{\mathrm{up.}}^{t}$ is the estimation of the upsampled intensity component after the tth iteration, and "υ" is the step size of the gradient descent. The result obtained through (16) is the final stage of estimating the upsampled intensity component. This component is close to the initial upsampled intensity component given by the local synthesis approach, as much as possible, whereas it is globally consistent with the intensity component.

IV. Experimental Results

In this letter, two data sets collected by the WorldView-2 and DEIMOS-2 sensors have been used to evaluate the proposed method. The scale ratio ρ is 4 for both data sets, and the number of spectral bands is 4 for DEIMOS-2 and 8 for WorldView-2.

To evaluate the fusion results, we use the Wald synthesis protocol [22]. According to this protocol, the LRM and HRP images are preliminarily decimated by the scale ratio, and therefore, reference LRM bands are available for comparisons. The pan-sharpened results are assessed by correlation coefficient (CC), universal image quality index (UIQI) [23], root-mean-square error (RMSE), spectral angle mapper (SAM) [24], and *Quality with No Reference* (QNR) index [25], which is composed of a *spectral distortion* D_λ index and a *spatial distortion* D_s index, without requiring a high-resolution reference multispectral image. The proposed nonlinear method is compared with the generalized IHS [2] method and the modified IHS method [19]. In order to have a balanced tradeoff between performance and computation time, we choose a patch size of [5 5] with overlap $r=40\%$. Parameters "γ" and "ε" in (5) are set as 10^{-9} and 10^{-10}, respectively, both for the modified IHS and the proposed nonlinear IHS. Parameter "λ" is set as 5 for the modified IHS method, where it achieves its best

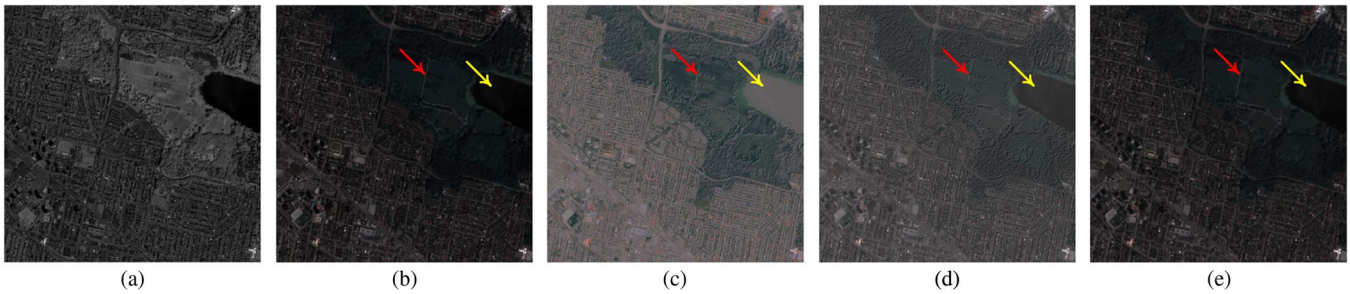

Fig. 2. Simulated experiments with the DEIMOS-2 data set. (a) Degraded HRP (512 × 512 and 4 m). (b) Reference LRM (512 × 512 and 4 m; RGB: bands 2, 3, and 4). (c) Generalized IHS. (d) Modified IHS. (e) Nonlinear IHS.

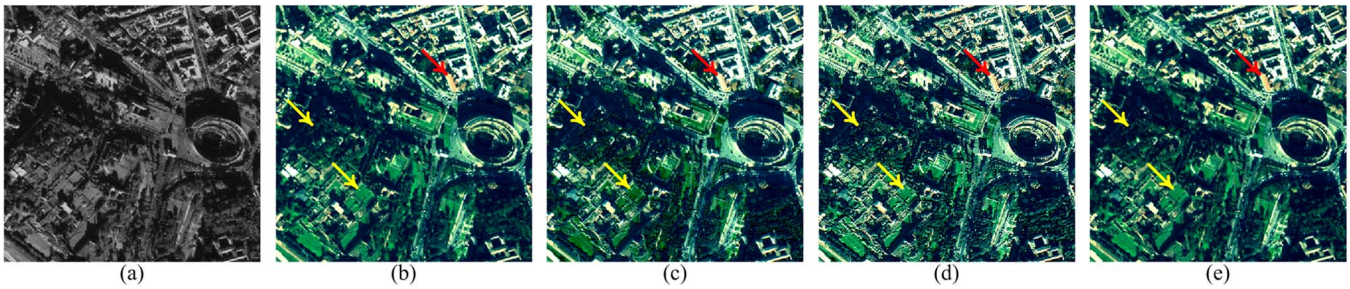

Fig. 3. Simulated experiment with the WorldView-2 data set. (a) Degraded HRP (512 × 512 and 1.84 m). (b) Reference LRM (512 × 512 and 7.36 m; RGB: bands 5, 3, and 2). (c) Generalized IHS. (d) Modified IHS. (e) Nonlinear IHS.

TABLE I
PERFORMANCE OF THE FUSION RESULTS

Methods	DEIMOS-2							WorldView-2						
	CC (Avg.)	RMSE (Avg.)	Q (Avg.)	SAM (deg.)	QNR			CC (Avg.)	RMSE (Avg.)	Q (Avg.)	SAM (deg.)	QNR		
					D_s	D_λ	Avg.					D_s	D_λ	Avg.
Reference Value	1	0	1	0	0	0	1	1	0	1	0	0	0	1
Generalized IHS	0.658	18.66	0.837	14.65	0.318	0.170	0.567	0.753	14.27	0.684	11.30	0.332	0.153	0.566
Modified IHS	0.782	10.63	0.875	10.06	0.253	0.103	0.670	0.839	11.40	0.703	08.85	0.324	0.107	0.603
Nonlinear IHS	0.948	04.84	0.967	03.64	0.130	0.045	0.831	0.968	03.27	0.751	02.14	0.218	0.027	0.761

performance. The MATLAB code and documentation of the proposed nonlinear IHS method are available online.[1]

Fig. 2 shows the pan-sharpened LRM results of the DEIMOS-2 data using different methods. Comparing the result of the generalized IHS method [see Fig. 2(c)] with the reference image [see Fig. 2(b)], it is clear that the method provides a high spatial resolution result, but this is unable to preserve the spectral information of the source image. As shown in Fig. 2(d), the modified IHS method maintains better spectral information than the generalized IHS method. However, this method introduces two types of distortions. The first is spectral distortion; as the region indicated by a yellow arrow shows, the spectral information of the modified IHS method's result is inconsistent with that of the reference image. The second is spatial distortion, i.e., the spatial details are also weak. For instance, the road indicated by a red arrow is an example of a weak spatial resolution result. The pan-sharpened result of our method is shown in Fig. 2(e). From this figure, it can be seen that the proposed nonlinear IHS method provides good result.

The experiments with the WorldView-2 data set are shown in Fig. 3. Comparing the pan-sharpening results with the reference image shown in Fig. 3(b), it is obvious that the oversharpening phenomena are substantially occurred in the results of the generalized [see Fig. 3(c)] and modified [see Fig. 3(d)] IHS methods; for instance, the spectral distortion in the vegetation areas indicated by yellow arrows is more severe in the result of the generalized IHS method than in that of the modified method. Aside from the spectral distortion in the edge regions, the generalized and modified IHS methods also introduce spectral distortion in the nonedge regions. The building indicated by a red arrow is an example of weak spectral preservation. Fig. 3(e) verifies that the spectral distortion in the result of our method is less.

The quantitative assessments of the pan-sharpened data shown in Figs. 2 and 3 are reported in Table I. As expected, the proposed method greatly improves the quality of the pan-sharpened content. The proposed method achieves the best performance in all the quantitative terms. The time costs for the experiments with the DEIMOS-2 and WorldView-2 data sets are reported in Table II. From the table, it can be seen that the proposed method requires more computation time than the other methods, which is mainly due to the patch-by-patch synthesis.

[1]http://openremotesensing.net/index.php/codes

TABLE II
TIME COSTS (IN SECONDS) OF THE DIFFERENT PAN-SHARPENING METHODS FOR THE 512 × 512 DATA (CENTRAL PROCESSING UNIT CORE I7 AND 6-GB RANDOM ACCESS MEMORY)

Methods	DEIMOS-2	WorldView-2
Generalized IHS	0.05	0.07
Modified IHS	0.39	0.4
Nonlinear IHS	2.55	2.6

V. CONCLUSION

In this letter, we have proposed a nonlinear IHS-based pan-sharpening method for reducing the spectral distortion. We have also proposed a new local–global framework to estimate the intensity component. This scheme could successfully provide stable weight vectors to approximate the intensity component. The empirical results show that the proposed approach remarkably reduces spectral and spatial distortions from the pan-sharpened results and provides consistent results with the reference data locally and globally. Overall, it can be said that, in this letter, we relax the linearity of the modified IHS to a nonlinearity of that.

ACKNOWLEDGMENT

The authors would like to thank DigitalGlobe and Deimos Imaging for acquiring and providing the data used in this study, the IEEE Geoscience and Remote Sensing Society Image Analysis and Data Fusion Technical Committee, and S. Rahmani for providing the software of the modified IHS method. They would also like to thank the Editor and the anonymous reviewers for their constructive comments.

REFERENCES

[1] M. Ghahremani and H. Ghassemian, "A compressed-sensing-based pan-sharpening method for spectral distortion reduction," *IEEE Trans. Geosci. Remote Sens.*, vol. 54, no. 4, pp. 2194–2206, Apr. 2016.

[2] T. M. Tu, S. C. Su, H. C. Shyu, and P. S. Huang, "A new look at IHS like image fusion methods," *Inf. Fusion*, vol. 2, no. 3, pp. 177–186, Sep. 2001.

[3] C. A. Laben and B. V. Brower, "Process for enhancing the spatial resolution of multispectral imagery using pan-sharpening," U.S. Patent 6 011 875, Jan. 4, 2000.

[4] P. S. Chavez, S. C. Sides, and J. A. Anderson, "Comparison of three different methods to merge multiresolution and multispectral data: Landsat TM and SPOT panchromatic," *Photogramm. Eng. Remote Sens.*, vol. 57, no. 3, pp. 295–303, Mar. 1991.

[5] J. Nunez, X. Otazu, O. Fors, A. Prades, V. Pala, and R. Arbiol, "Multiresolution-based image fusion with additive wavelet decomposition," *IEEE Trans. Geosci. Remote Sens.*, vol. 37, no. 3, pp. 1204–1211, May 1999.

[6] M. Ghahremani and H. Ghassemian, "Remote sensing image fusion based on curvelets and ICA," *Int. J. Remote Sens.*, vol. 36, no. 16, pp. 4131–4143, Aug. 2015.

[7] M. Choi, R. Y. Kim, M. R. Nam, and H. O. Kim, "Fusion of multispectral and panchromatic satellite images using the curvelet transform," *IEEE Geosci. Remote Sens. Lett.*, vol. 2, no. 2, pp. 136–140, Apr. 2005.

[8] M. Ghahremani and H. Ghassemian, "Remote sensing image fusion using ripplet transform and compressed sensing," *IEEE Geosci. Remote Sens. Lett.*, vol. 12, no. 3, pp. 502–506, Mar. 2015.

[9] L. Zhang, H. Shen, W. Gong, and H. Zhang, "Adjustable model-based fusion method for multispectral and panchromatic images," *IEEE Trans. Syst., Man, Cybern. B, Cybern.*, vol. 42, no. 6, pp. 1693–1704, Dec. 2012.

[10] M. V. Joshi, L. Bruzzone, and S. Chaudhuri, "A model-based approach to multiresolution fusion in remotely sensed images," *IEEE Trans. Geosci. Remote Sens.*, vol. 44, no. 9, pp. 2549–2562, Sep. 2006.

[11] S. Li and B. Yang, "A new pan-sharpening method using a compressed sensing technique," *IEEE Trans. Geosci. Remote Sens.*, vol. 49, no. 2, pp. 738–746, Feb. 2011.

[12] C. Jiang, H. Zhang, H. Shen, and L. Zhang, "Two-step sparse coding for the pan-sharpening of remote sensing images," *IEEE J. Sel. Topics Appl. Earth Observ. Remote Sens.*, vol. 7, no. 5, pp. 1792–1805, May 2014.

[13] C. Thomas, T. Ranchin, L. Wald, and J. Chanussot, "Synthesis of multispectral images to high spatial resolution: A critical review of fusion methods based on remote sensing physics," *IEEE Trans. Geosci. Remote. Sens.*, vol. 46, no. 5, pp. 1301–1312, May 2008.

[14] L. Gomez-Chova, D. Tuia, G. Moser, and G. Camps-Valls, "Multimodal classification of remote sensing images: A review and future directions," *Proc. IEEE*, vol. 103, no. 9, pp. 1560–1584, Sep. 2015.

[15] H. Ghassemian, "A review of remote sensing image fusion methods," *Inf. Fusion*, vol. 32, no. 9, pp. 75–89, Nov. 2016.

[16] T. M. Tu, P. S. Huang, C. L. Hung, and C. P. Chang, "A fast intensity–hue–saturation fusion technique with spectral adjustment for IKONOS imagery," *IEEE Geosci. Remote Sens. Lett.*, vol. 1, no. 4, pp. 309–312, Oct. 2004.

[17] M. Choi, "A new intensity–hue–saturation fusion approach to image fusion with a tradeoff parameter," *IEEE Trans. Geosci. Remote Sens.*, vol. 44, no. 6, pp. 1672–1682, Jun. 2006.

[18] M. C. El-Mezouar, N. Taleb, K. Kpalma, and J. Ronsin, "An IHS-based fusion for color distortion reduction and vegetation enhancement in IKONOS imagery," *IEEE Trans. Geosci. Remote Sens.*, vol. 49, no. 5, pp. 1590–1602, May 2011.

[19] S. Rahmani, M. Strait, D. Merkurjev, M. Moeller, and T. Wittman, "An adaptive IHS pan-sharpening method," *IEEE Geosci. Remote Sens. Lett.*, vol. 7, no. 4, pp. 746–750, Oct. 2010.

[20] Y. Leung, J. Liu, and J. Zhang, "An improved adaptive intensity–hue–saturation method for the fusion of remote sensing images," *IEEE Geosci. Remote Sens. Lett.*, vol. 11, no. 5, pp. 985–989, May 2014.

[21] G. H. Golub and C. F. Van Loan, *Matrix Computations*. Baltimore, MD, USA: The Johns Hopkins Univ. Press, 2013, pp. 313–317.

[22] T. Ranchin and L. Wald, "Fusion of high spatial and spectral resolution images: The ARSIS concept and its implementation," *Photogramm. Eng. Remote Sens.*, vol. 66, no. 1, pp. 49–61, Jan. 2000.

[23] L. Alparone, B. Aiazzi, S. Baronti, A. Garzelli, and P. Nencini, "A global quality measurement of pan-sharpened multispectral imagery," *IEEE Geosci. Remote Sens. Lett.*, vol. 1, no. 4, pp. 313–317, Oct. 2004.

[24] R. H. Yuhas, A. F. H. Goetz, and J. W. Boardman, "Discrimination among semi-arid landscape endmembers using the Spectral Angle Mapper (SAM) algorithm," in *Proc. Summaries 3rd Annu. JPL Airborne Geosci. Workshop*, 1992, pp. 147–149.

[25] L. Alparone, B. Aiazzi, S. Baronti, A. Garzelli, F. Nencini, and M. Selva, "Multispectral and panchromatic data fusion assessment without reference," *Photogramm. Eng. Remote Sens.*, vol. 74, no. 2, pp. 193–200, Feb. 2008.